Available online at www.sciencedirect.com
SCIENCE DIRECT®
Journal of Nuclear Materials 337–339 (2005) 771–775
journal of nuclear materials
www.elsevier.com/locate/jnucmat

ELM-induced plasma transport in the DIII-D SOL

J.A. Boedo [a,*], D.L. Rudakov [a], E.M. Hollmann [a], R.A. Moyer [a], G.R. McKee [b], K. Burrell [c], T.E. Evans [c], A.W. Leonard [c], W.P. West [c], M.E. Fenstermacher [d], M. Groth [d], S.L. Allen [d], L. Zeng [e], G. Wang [e], J.G. Watkins [f], The DIII-D Team [a]

[a] *Center for Energy Research Eng., University of California, Building Unit II, Rm 460 9500, Gilman Dr La Jolla, San Diego, CA 92093-0417, USA*
[b] *University of Wisconsin, Madison, WI 53706, USA*
[c] *General Atomics, P.O. Box 85608, San Diego, CA 92186-5608, USA*
[d] *Lawrence Livermore National Laboratory, Livermore, CA 94550, USA*
[e] *University of California Los Angeles, Los Angeles 90032, CA, USA*
[f] *Sandia National Laboratories, Albuquerque, NM 87123, USA*

Abstract

High temporal and spatial resolution measurements in the boundary of the DIII-D tokamak show that edge localized modes (ELMs) are composed of fast bursts of hot, dense plasma lasting ~25 μs each that travel radially starting at the separatrix at ~450 m/s and rotate in the scrape off layer (SOL), convecting particles and energy to the SOL and walls. The temperature and density in the ELM plasma initially correspond to those at the top of the density pedestal but decay with radius in the SOL. The temperature decay length (~1.2–1.5 cm) is much shorter than the density decay length (~3–8 cm), which in turn decreases with increasing pedestal density. The local particle and energy flux at the wall during the bursts are 10–50% (~$1–2\times10^{21}$ m^{-2} s^{-1}) and 1–2% (~20–30 kW/m^2) respectively of the LCFS average fluxes, thus particles are transported radially much more efficiently that heat.

PACS: 52.40.Hf; 52.35.Ra; 52.55.FA; 52.70.Ds
Keywords: DIII-D; Edge Plasma; Cross-field transport; Intermittent transport

1. Introduction

High performance tokamak discharges operate in ELMing H-mode to combine high-energy confinement with adequate particle exhaust. However, the ELM instability also carries a considerable amount of particles and heat from the pedestal region into the SOL towards the divertor region and other plasma facing components (PFCs), possibly limiting their lifetime and causing the release of impurities into the plasma. According to accepted scalings, type I ELMs could exceed the ITER PFC damage threshold [1] resulting in a divertor lifetime of less than one full discharge. Therefore, it is important to invest a significant effort to study ELMs the ELM

* Corresponding author. Address: UCSD, 9500 Gilman Dr, La Jolla, CA 92093-0417, USA. Tel.: +1 858 455 2832; fax: +1 858 455 2266.
E-mail address: jboedo@ucsd.edu (J.A. Boedo).

0022-3115/$ - see front matter © 2004 Elsevier B.V. All rights reserved.
doi:10.1016/j.jnucmat.2004.10.159

dynamics in the SOL in order to envision ways of controlling their interaction with the PFCs.

A number of theoretical studies [2] of ELMs have emphasized the linear regime of dominant modes [3] referred to as coupled 'peeling-ballooning' modes, are driven by both parallel current (J_{ped}) and the pressure gradient (p'_{ped}). These intermediate-n peeling-ballooning modes, whose linear phase can be calculated using the ELITE code, impose limits on the pedestal height, which are functions of the pedestal width, plasma shape, collisionality, safety factor and other equilibrium details. Preliminary nonlinear studies [4,5] suggest that during the ELM, filaments will grow in the pedestal region and travel across the separatrix into the SOL, carrying particles and heat with them. This paper provides information on ELM structure and propagation that can be used to improve the models.

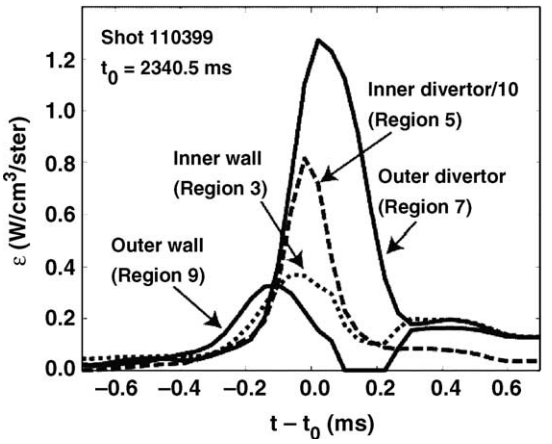

Fig. 1. Inversion of DISRAD2 data from a single ELM (Type I) shows radiation peaking first in the outer SOL then in the inner SOL, later at the divertor regions.

2. Experimental setup

Experiments to characterize ELMs on the DIII-D tokamak [6] were carried out in H-mode discharges featuring type I ELMs with plasma current $I_p = 1.4$ MA, toroidal field of $B_T = 1.7$ T at the axis, $R = 1.7$ m and neutral beam heating power of up to 4.5 MW. Lower single-null divertor geometry with ion Grad-B drift toward the lower divertor was used. The density was increased in a sequence of discharges, from $\langle n_e \rangle / n_G = 0.40$–$0.8$. ($n_G$ is the Greenwald limit) The principal measurements were made by the fast radiometer array [7] (DISRAD2), a fast scanning probe, [8] Beam emission spectroscopy [9] (BES), reflectometry [10] and charge exchange recombination spectroscopy, CER [11]. The fast scanning probe array features five tips that sense current, I, saturation current, I_{sat}, and floating potential, Φ_f. A ≈ 250 kHz bandwidth T_e measurement [12] is used to resolve the temperature inside the ELMs. The BES system, configured as a 5×6 fiber array, was located at the edge of the plasma in the midplane to provide fast (1 μs) 2-D imaging of the density. The DISRAD2 measures absolutely calibrated photon intensity along 30 poloidally separated view chords at a rate of 100 kHz and a photon energy response of 1 eV–5 keV.

Inversion of the DISRAD2 data (Fig. 1) shows the integrated ELM radiation for various plasma regions as a function of time measured from the beginning of an arbitrary ELM, or t_0. The radiation rises first on the outer SOL indicating low field side ELM formation, it then rises in the inner SOL and thereafter in the divertor. Two frames from BES taken at an arbitrary time near an ELM onset, t_0^{BES} and 16 μs later ($t_0^{BES} + 16$ μs) and shown in Fig. 2, feature an ELM as a positive density feature appearing at the bottom of the frame and moving upward to the center. The data shown is the

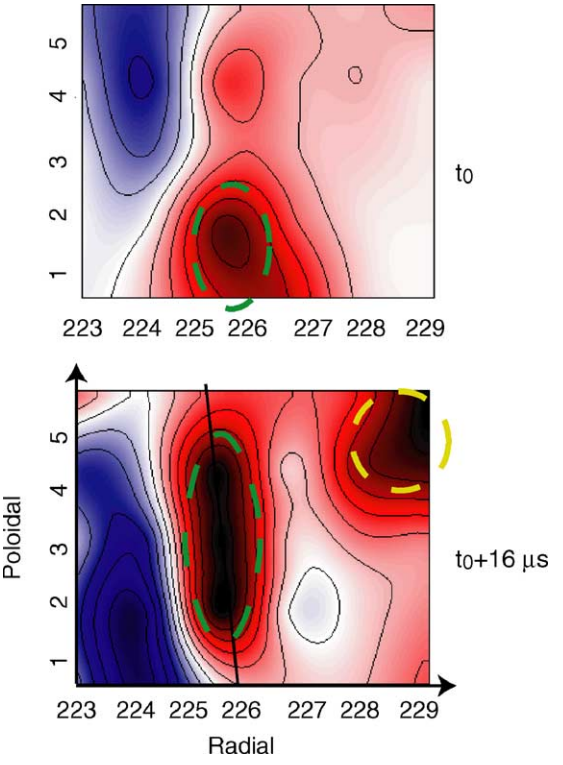

Fig. 2. Frames from BES showing 2-D density plots with exposure of 1 μs. The Type I ELM is seen at t_0 at the bottom of the top frame (green ellipse). A second frame (bottom) is taken 16 μs thereafter, showing the initial ELM structure (green ellipse) moving upward (poloidally) and an ejection on the upper right (dashed yellow circle) that has moved radially. (For interpretation of the references in color in this figure legend, the reader is referred to the web version of this article).

deviation from the average value and in the color scheme, white represents average (or background) density and red and blue represent positive and negative fluctuations, black indicates saturation. The LCFS is indicated by a solid vertical line. The ELM includes plasma ejections produced near the separatrix that then move radially at nearly 7 km/s (the BES measurements were made in a different set of discharges that those otherwise discussed in this paper). Probe measurements of $V_r = E_\theta B/B^2$ and reflectometry [13] data show the ELM radial velocity peaking at ~500 m/s at the LCFS and and decaying to 120 m/s in the SOL.

The ELMs can then be seen as filamentary structures with complex spatial and temporal time structure [14], consistent with BES data, that is observed as multiple bursts in the temperature and density data taken by probes, shown in Fig. 3. The high time resolution data, displayed in a 12 ms window that arbitrarily spans the ELM duration. The ELM plasma features peak n_e values (first peak in the series of bursts per ELM) corresponding to those at the top of the density pedestal ($\sim 3 \times 10^{19}$ m^{-3}) if the spatial decay is accounted for, suggesting that the ELM peels off from the top of the density pedestal. The ELM peak density and temperature decay with distance from the LCFS due to parallel transport [15] and the decay varies with density as shown in Fig. 4. At high n_e ($n_e/n_G = 0.85$) the density decay length, L_N~3.8 cm while the temperature decay length, L_T is ~1.2 cm. At $n_e/n_G = 0.45$, L_N and L_T are 13 cm and 1.3 cm, respectively. The particles in the ELM travel essentially unhindered towards the wall at low densities while at high density, the particles are quickly dissipated. The heat in the ELM is dissipated rapidly with radius, irrespective of the pedestal density consistently with IR camera results, which see a broadening of the heat and particle flux divertor plate profiles during ELMs [16].

Based on measurements of ELM convection speeds, the wall (6 to 7 cm from the LCFS) would be stricken in roughly 0.3 ms for these discharges. The ***local*** burst peak heat and particle radial flux convected by the ELM towards the wall are $\Gamma_r = nV_r$ and $Q_r = 2 \times 3/2nTV_r$ respectively. The ELM-induced ***local*** convected radial heat flux at the LCFS due to the bursts is ~80% of the average (calculated as $(P_{in}–P_{rad})$/Area) at the LCFS, at $\langle n_e \rangle / n_{GW} = 0.8$ and ~60% at $\langle n_e \rangle / n_{GW} = 0.45$. However, the heat flux reaching the wall, shown in Table 1, is only a ~2% fraction of the LCFS heat flux, consistently with the short (~1.5 cm) T_e radial decay, thus

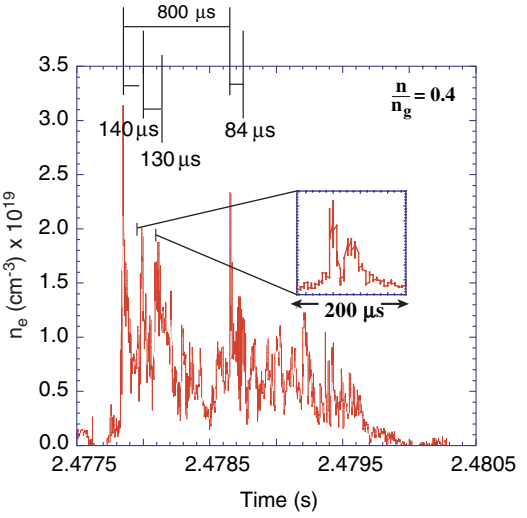

Fig. 3. Probe density data for a low discharge density ($n/n_g = 0.4$) at $R–R_{sep} = 1.5$ cm. The density bursts last ~30 μs, initially appearing at regular intervals (~140 μs). The intervals can show gaps of ~300–400 μs between groups of bursts. The inset shows a burst detail.

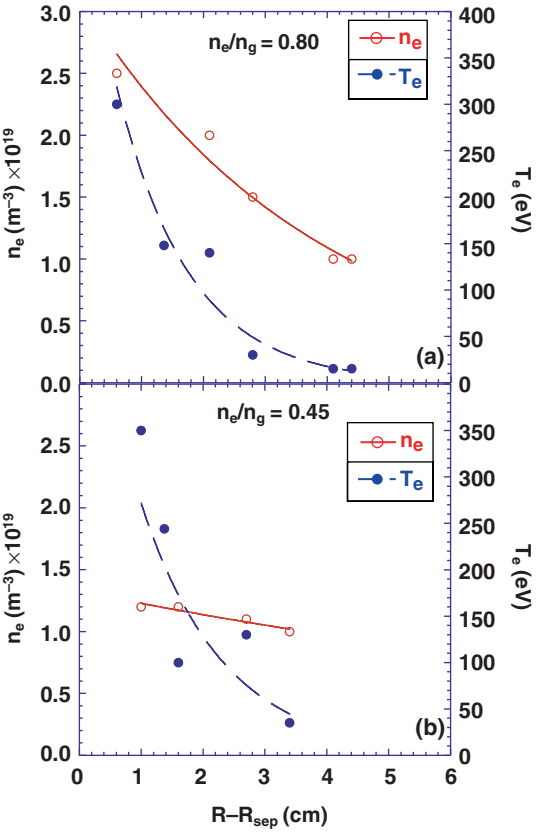

Fig. 4. Radial variation of the ELM ***burst*** peak density and temperature values obtained from probes for (a) high density and (b) low density discharges. The temperature decays quickly with radius in both cases, but the density decay length is much longer at low density.

Table 1
Radial particle (Γ_r^{ELM}) and heat (Q_r^{ELM}) fluxes due to an ELM at the LCFS and the wall for low density $\langle n_e\rangle/n_{GW} = 0.45$ high density $\langle n_e\rangle/n_{GW} = 0.8$ discharges

$\langle n_e\rangle/n_{GW} = 0.8$	Γ_r^{ELM} ($m^{-2}\,s^{-1}$)	Q_r^{ELM} ($J\,m^{-2}\,s^{-1}$)
LCFS	1.0×10^{22}	1 800 000
Wall	1.5×10^{21}	21 600
$\langle n_e\rangle/n_{GW} = 0.45$	Γ_r^{ELM} ($J\,m^{-2}\,s^{-1}$)	Q_r^{ELM} ($J\,m^{-2}\,s^{-1}$)
LCFS	5.6×10^{21}	1 323 000
Wall	1.8×10^{21}	27 000

most of the heat flux is transported along the magnetic field and strikes the divertor floor. The local convected radial particle flux due to the ELM bursts at the wall is 10–50% of the LCFS local average radial flux, or $\sim1.6\times10^{21}\,m^{-2}\,s^{-1}$, consistent with the long density decay length (~3–8 cm). Table 1 indicates that the ELM local peak particle flux at the wall is similar for all densities due to the fact that at higher pedestal densities the ELM plasma density increases but the decay length becomes shorter.

3. Interpretations of the ELM dynamics data

Assuming mainly radial motion of the ELMs and using the measured radial ELM velocity, V_r, at the LCFS (~450 m/s), the radial extent of each burst is estimated as $\delta r = V_r \times \delta t$, where δt is the duration of the pulse. Radial extents of 2–5 cm per burst are obtained from the burst duration (~20–40 μs long). Gaps lasting ~130–140 μs are seen between bursts, sometimes followed by a longer gap of ~800 μs between trains of bursts. Therefore, the ELM comes from the LCFS in well-defined bursts that substantially fill the SOL (6–7 cm gap) with dense plasma. This paradigm, however, is hard to reconcile with the fact that many diagnostics in all toroidal and poloidal locations see the ELM promptly within a small time delay of ~100 μs.

Another possibility is that the ELM plasma is also rotating toroidally. The CER [11] toroidal speeds during an ELM at radii straddling the LCFS are shown, together with a rotation profile (Fig. 5(b) before (t_0–1 ms) and during (t_0) an ELM, where t_0 is determined by the rise of the fast D_α signal in the divertor. The onset of

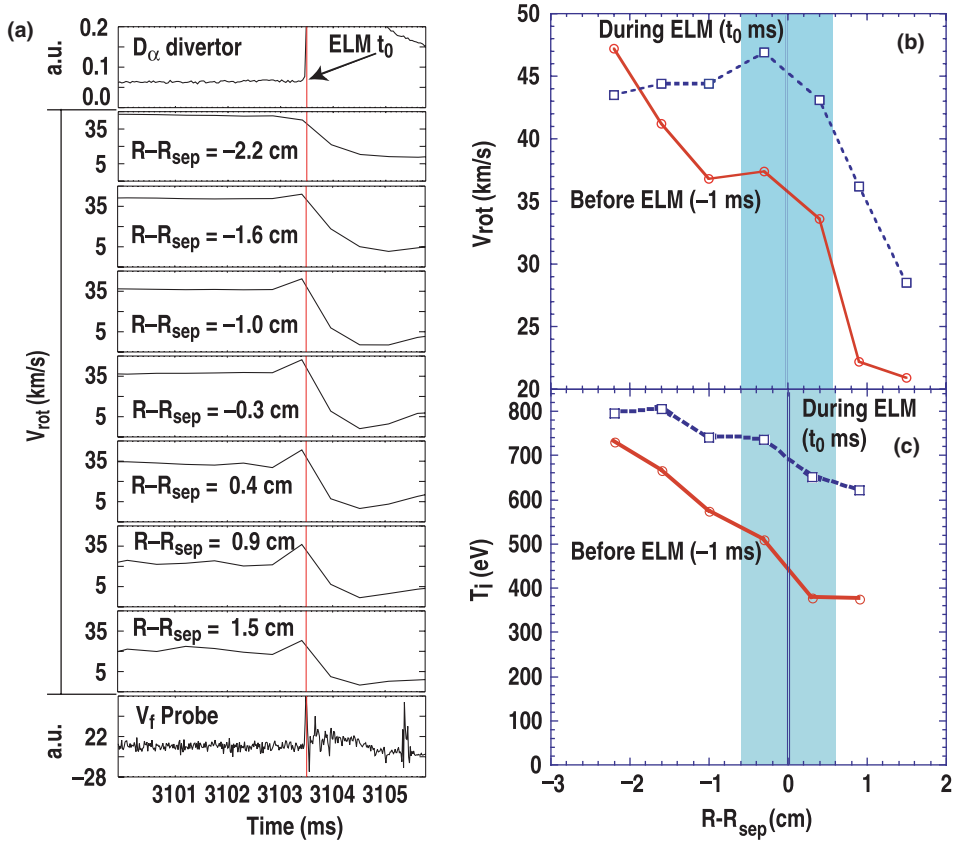

Fig. 5. (a) CER data showing a profile of the toroidal rotation velocity of carbon ions. A floor D_α signal [(a) top] is used as a fiducial. Profiles of rotation velocity (b) and ion temperature (c) taken during the ELM ($t = 0$) and before the ELM ($t = -1$ ms). The shaded region indicates uncertainty in the EFIT.

an ELM is concomitant with a transient increase of toroidal velocity and ion temperature (all from carbon) further out and into the SOL (Fig. 5(b) and (c), which lasts $\ll$1 ms, consistent with the radial ELM plasma travel time ($\sim$0.3 ms). The peak toroidal velocity and ion temperature of the radial transient corresponds to that of the innermost chord pre-ELM velocity, supporting that ELMs originate at the top of the pedestal. The CER-measured toroidal velocity is $\sim$30 km/s in the SOL, corresponds to $\sim$650 μs period, longer than the expected ELM plasma radial travel time of 200–300 μs, so the ELM plasma does not have time to rotate fully before hitting the wall. Once the rotation assumption is considered, Fig. 3 can be re-examined. The initial density bursts are separated by $\sim$135 μs, followed by a $\sim$450 μs gap before the bursts start again. Therefore, this sequence could be interpreted as three filaments (multiple n, m structures) rotating by the probe and returning with a period $T = 800$ μs while decaying by parallel transport.

Acknowledgments

This research was supported by the US Department of Energy under Contract Nos. DE-FC02-04ER54698, W-7405-ENG-48, DE-AC05-76OR00033, DE-AC04-94AL85000 and Grant Nos. DE-FG03-95ER54294, DE-FG03-96ER54373, DE-FG03-01ER54615, DE-AC04-94AL8500. The technical support of L. Chousal and R. Hernandez are acknowledged.

References

[1] H.D. Pacher et al., ITER Design Description Document, ITER No. G 17 DDD 1 96-08-21 W2.1, 1996.
[2] J.W. Connor, R.J. Hastie, H.R. Wilson, R.L. Miller, Phys. Plasmas 5 (1998) 2687.
[3] P.B. Snyder, H.R. Wilson, J.R. Ferron, L.L. Lao, A.W. Leonard, T.H. Osborne, A.D. Turnbull, D. Mossessian, M. Murakami, X.Q. Xu, Phys. Plasmas 9 (2002) 2037.
[4] P.B. Snyder, X. Xu, private communication, 2004.
[5] S. Cowley, H. Wilson, et al., PPCF 45 (2003) A31.
[6] J.L. Luxon, Nucl. Fusion 42 (2002) 614.
[7] D.S. Gray, S.C. Luckhardt, A.G. Kellman, et al., Rev. Sci. Instrum, submitted for publication.
[8] J. Watkins, J. Salmonson, R. Moyer, et al., Rev. Sci. Instrum. 63 (1992) 4728.
[9] R.J. Fonck, G. Cosby, R.D. Durst, S.F. Paul, N. Bretz, S. Scott, E. Synakowski, Phys. Rev. Lett. 70 (1993) 3736.
[10] T.L. Rhodes, S. Baang, A.E. Chou, C.W. Domier, N.C. Luhmann, Jr., W.A. Peebles, Rev. Sci. Instrum. 63 (1992) 4599.
[11] K.H. Burrell, Rev. Sci. Instrum. 72 (2001) 906.
[12] D.L. Rudakov, J.A. Boedo, R.A. Moyer, et al., Rev. Sci. Instrum. 72 (2001) 453.
[13] L. Zeng, E.J. Doyle, T.L. Rhodes, G. Wang, W.A. Peebles, K.H. Burrell, Rev. Sci. Instrum. 74 (2003) 1530.
[14] T. Eich, PRL, 91-19 (2003) 5003.
[15] D.A. D'Ippolito, J.R. Myra, S.I. Krasheninnikov, Phys. Plasmas 9 (2002) 222.
[16] A.W. Leonard, W. Suttrop, T.H. Osborner, et al., J. Nucl. Mater. 241–243 (1997) 628.